CA-2 | 71

ASAT

MILITARY TECHNICAL COLLEGE
CAIRO - EGYPT

MODELLING COMPRESSIBLE FLOW IN AXISYMMETRIC DUCTS OF VARYING CROSS-SECTIONAL AREA

Wafik A. Kamal* , Anwar E.M. Anwar**

ABSTRACT

A theoretical model of the flow in 3-D axisymmetric ducts with high subsonic intake Mach numbers is developed. The model is based on the iteration between the axisymmetric potential core flow and a proven compressible turbulent boundary layer method based on the entrainment principle. The solution of the core flow partial differential equations is achieved through expanding both the stream function and the density function as power series of the duct radius thus reducing them to a series of linear simultaneous ordinary differential equations. The boundary layer method is capable of handling excessively disturbed inlet flows, by accounting for upstream history effects on the boundary layer development. A single integral parameter is used to describe the inlet turbulence structure. The model is verified using experimental data available in the literature, and the verification proved its success in predicting the pressure recovery of the intake system and its sensitivity to variations in inlet flow and geometrical parameters.

---

* Associate Professor, Alexandria University, Egypt (Currently on leave to Qatar University), ** Graduate student, Alexandria University (Lt. Colonel, Air Force).

INTRODUCTION

Complex three-dimensional ducts are in evidence in numerous engineering applications ranging from air conditioning system ducts and high speed centrifugal compressor diffusers to aircraft intake and gas turbine transition ducts.

In the past gas turbine engine transition ducts, for example, were considered to perform little more than transporting the working fluid from one engine component to the next. However, with the ever increasing cost of fuel and with the advent of high by-pass ratio engines, the intercomponent duct has been forced to the fore as designers strive to reduce losses in the overall system. It is clear then that the accurate prediction of total pressure loss, of the boundary layer developement through the duct and of the variation of the these parameters with inlet conditions now form the basic requirements of any satisfactory duct design method.

Although the last decade has witnessed the development of few elaborate schemes for the calculation of general three-dimensional internal flows - references [1], [2] & [3] - we believe that there is still room for a relatively simple prediction procedure restricted to axisymmetric compressible duct flows free from complex 3-D phenomena like separation, cavitation and boundary layers merging.

The present method iterates an inviscid irrotational 3-D axisymmetric core flow solution [4] with a proven compressible turbulent boundary layer method [5]. The potential flow model proved its success in handling ducts with gradually or sharply varying cross sections (expansions or contractions). On the other hand the boundary layer method is designed for ducts with high inlet turbulence levels, sufficiently high to influence the flow regimes in the ducts and in particular in diffusing sections.

The model predictions are compared to experimental data for conical diffusers preceded and followed by sections of parallel pipes with the transition from the inlet pipe to the diffuser cone being faired [6] & sharp [7]. The data used for the comparison from ref. [6] are for diffusers preceded by wholly subsonic flow while those from ref. [7] are for diffusers preceded by shock wave - boundary layer interactions in the inlet pipe.

THE THEORETICAL MODEL

Basic Assumptions

i- A steady 3-D axisymmetric isentropic core flow extends to the duct exit, i.e., the boundary layers do not merge.
ii- The boundary layers are adiabatic, thin at duct inlet, growing on a smooth wall under ordinary rates of strain.
iii- The flowing fluid is a perfect gas.

The Prediction Scheme

The solution for the duct wall pressure distribution and total pressure

loss as well as the variation of boundary layer parameters along the duct is obtained in three steps:-

i- Solving the potential duct flow partial differential equations by an approximate method. This consists of expanding each of the stream function and the density function as a power series in terms of the radius, thus reducing the inviscid flow equations to a series of simultaneous ordinary differential equations. The duct is divided by a number of points along its axis and the derivatives replaced by a finite difference representation. The resulting linear simultaneous algebraic equations are solved using an elemination algorithm.

ii- Solving the boundary layer equations for the displacement thickness δ^* along the duct corresponding to the pressure distribution obtained from (i).

iii- Resolving the potential flow equations with a modified wall shape to take account of the boundary layer displacement.

Steps (ii) & (iii)are then repeated until the pressure distribution has converged to steady values.

Formulation of Equations for the Potential Core Flow

For a compressible potential axisymmetric core flow the irrotationality equation can be writen as [4]

$$RB\frac{\partial^2\psi}{\partial R^2}+\frac{\partial^2\psi}{\partial X^2}-R\left[\frac{\partial B}{\partial R}\cdot\frac{\partial \psi}{\partial R}+\frac{\partial B}{\partial X}\right]-B\cdot\frac{\partial\psi}{\partial R}=0 \qquad (1)$$

where

ψ is axisymmetric stream function defined using the boundary conditions $\psi = 0$ on the axis & $\psi = 1$ on the duct wall (see fig. 1).

B is the density function defined as

$$B = \rho / \rho_o \qquad (2)$$

For an incompressible flow, equation (1) reduces to

$$\frac{\partial^2\psi}{\partial X^2}+\frac{\partial^2\psi}{\partial R^2}-\frac{1}{R}\cdot\frac{\partial\psi}{\partial R}=0 \qquad (3)$$

which is Laplace's equation in cylindrical coordinates.

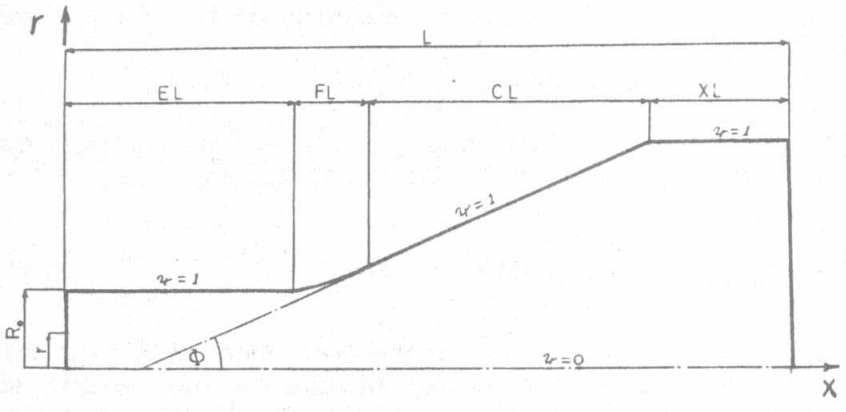

FIG (1) GENERAL DUCT GEOMETRY

Equation (1) is an elliptic partial differential equation and as such requires that either values of ψ or its derivatives be known at all points on a closed boundary. This is achieved by stipulating uniform flow in the axial direction at both entry and exit, ψ varying parabolically across the duct at either end between the values zero and one.

For a potential adiabatic (isentropic) axisymmetric flow the energy equation can be writen as

$$B^{\gamma-1} + \frac{\gamma-1}{2} M_o^2 \cdot \frac{1}{(2RB)^2} \left[\left(\frac{\partial \psi}{\partial R} \right)^2 + \left(\frac{\partial \psi}{\partial X} \right)^2 \right] = 1 + \frac{\gamma-1}{2} M_o^2 \qquad (4)$$

The introduction of power series for the stream function ψ and the compressibility function B allows the equations to be solved using direct elimination via a finite difference scheme. $\psi(X,R)$ & $B(X,R)$ are expanded as the following power series:

$$\psi(X,R) = R^2 . f_1(X) + R^4 . f_2(X) + R^6 . f_3(X) + \ldots\ldots\ldots \qquad (5)$$

$$B(X,R) = g_1(X) + R^2 . g_2(X) + R^4 . g_3(X) + \ldots\ldots\ldots \qquad (6)$$

Note here that the term $B^{\gamma-1}$ in equation (4) can be expanded in a binomial series as

$$B^{\gamma-1} = [1+(B-1)]^{\gamma-1}$$
$$= 1 + (\gamma-1)(B-1) + \frac{(\gamma-1)(\gamma-2)}{2} (B-1)^2 + \ldots\ldots\ldots \qquad (7)$$

Then B is subtituted from (6) into (7) before subtituting into equation (4). After the substitution (see reference [8]), it is found that all terms of the equation contain R^{2n} while the right hand side of the equation is zero. Therefore, the coefficients of R^{2n} must be zeros. This yields

$$\sum_{i=1}^{n} \left[\varepsilon(n+1-i) \sum_{j=1}^{i} (g_{i+1-j} \cdot g_j) \right] - (1+w) \left[\sum_{i=1}^{n} (g_i \, g_{n+1-i}) \right]$$
$$+ \frac{w}{4} \left[\sum_{i=1}^{n-1} (f'_i \cdot f'_{n-1}) + 4 \sum_{i=1}^{n-1} i(n-i+1) \, f_i \cdot f_{n-i+1} \right] = 0 \qquad (8)$$

where $w = (\gamma - 1) M_o^2/2$
and $\varepsilon(n)$ is the coefficient of R^{2n} in the expansion of $B^{\gamma-1}$, given in reference [8].
and the Dash ' denotes differentiation with respect to X.

Similarly when the power series, equations (5) & (6), are substituted in the irrotationality equation (1) and the coefficients of R^{2n+1} are equated to zero, we obtain

$$\sum_{j=1}^{n} (g'_j \cdot f'_{n+1-j} - g_j \cdot f''_{n+1-j}) + \sum_{j=1}^{n+1} [4(n+2-j)(2(j-1)-n) \, g_j \cdot f_{n+2-j}] = 0 \qquad (9)$$

In both equations (8) & (9) the derivatives (in the X-direction) are replaced by their finite difference representation using Taylor series expansion. It is the solution of these two sets of equations, in finite difference form, together with the boundary condition that $\psi = 1$ on the wall, which gives the values of f_i & g_i for the stream function and

6

density function in their respective power series expansions.

For a detailed account of the finite difference scheme as well as the iterative method of solving for the potential core pressure gradient, see ref. [8].

Formulation of the Boundary Layer Equations

In this analysis the boundary layer method developed by Kamal [5] is employed. The method is based on the simultaneous solution of three equations for the boundary layer with the free stream velocity U being fed from the potential core flow solution. The boundary layer equations are :

1- The momentum integral equation:

For a compressible axisymmetric boundary layer it takes the form :

$$\frac{d\theta}{dx} + \theta\left[(2+H-M_e^2)\frac{d(\ln U)}{dx} + \frac{d(\ln R)}{dx}\right] = \frac{C_f}{2} + \frac{1}{\rho_e U^2}\cdot\frac{d}{dx}\int_0^{\delta}(\rho\,\overline{v'^2} - \rho\,\overline{u'^2})dy \qquad (10)$$

For the skin friction C_f a modified version of the Ludwig-Tillman correlation was used, while for the Reynold's normal stress term (last term in equation 10, three different correlations were attempted [5].

2. The Entrainment Equation

A compressible form of Head's entrainment equation can be written as:

$$H_1\frac{d\theta}{dx} + \theta\frac{dH_1}{dx} = F - H_1\cdot\theta\left[(1-M_e^2)\frac{1}{U}\frac{dU}{dx} + \frac{1}{R}\frac{dR}{dx}\right] \qquad (11)$$

where $H_1 = 3.3 + 0.9/(\bar{H}-1)^{1.333}$

and $\bar{H} = (H+1)/(1+\frac{\gamma-1}{2}\,r_e\,M_e^2) - 1$ (r_e= temp. recovery factor)

3. The Boundary Layer History Equation

The turbulent kinetic energy integral equation is used to determine the streamwise evolution of the entrainment function F, thus

$$H_1\cdot\theta\left[\frac{1}{F}\frac{dF}{dx} + \frac{1}{U}\frac{dU}{dx} - \frac{1}{2R}\frac{dR}{dx}\right] = K_3\sqrt{C_f/2} - F/2 \qquad (12)$$

The value of $K_3 = 0.14$ is suggested.
(For the derivation of the above equations as well as a fuller account of the boundary layer model see references [5] & [7])

The 3 boundary layer equations constitute a system of first order differential equations in θ, H and the the turbulence determined entrainment function F. Once θ & H are determined, the boundary layer displacement thickness δ^* is calculated, the boundaries of the potential core are modified, and a new iteration is started until convergence is obtained.

An earlier attempt [4] to solve this set of boundary layer equations with the 3-D core flow model failed due to ill-conditioning of the boundary layer equations. For numerical stability of the Runge-Kutta method, the

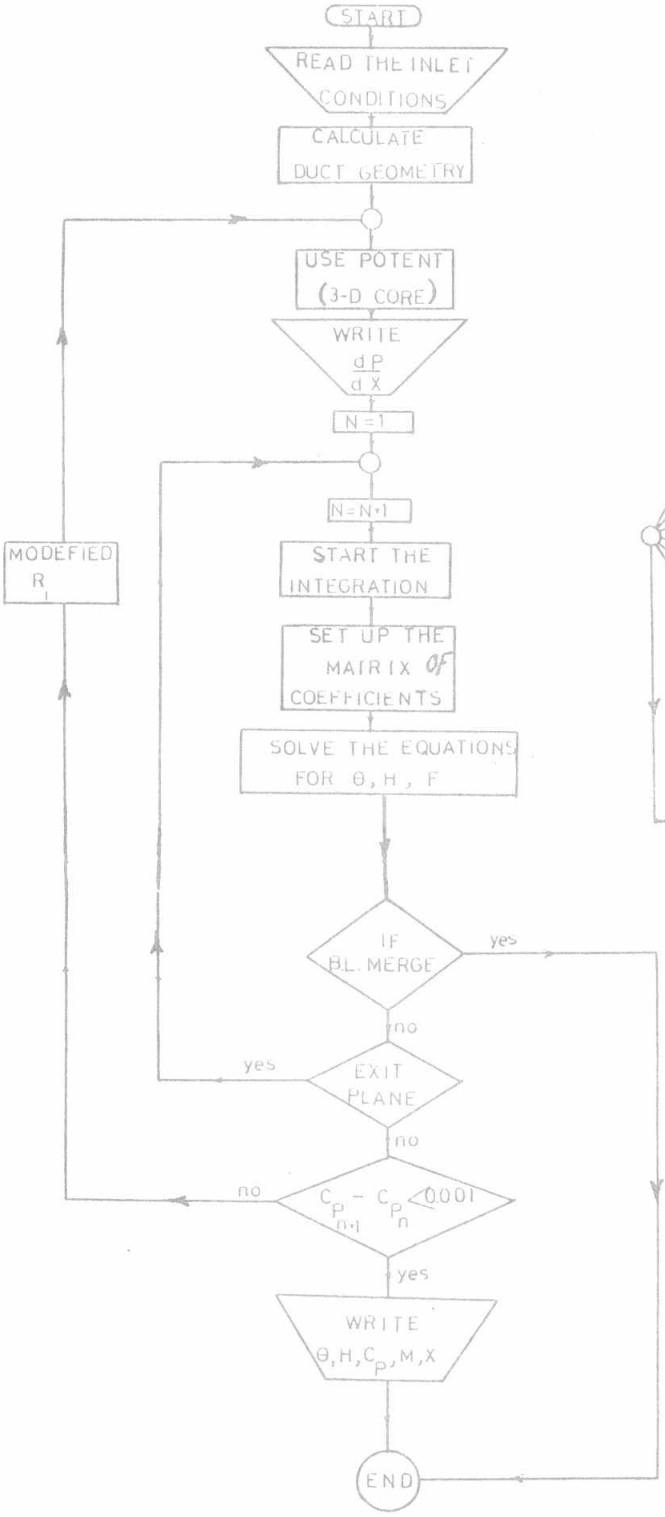

FIG 2 FLOWCHART DIAGRAM OF PROGRAM "DUCT"

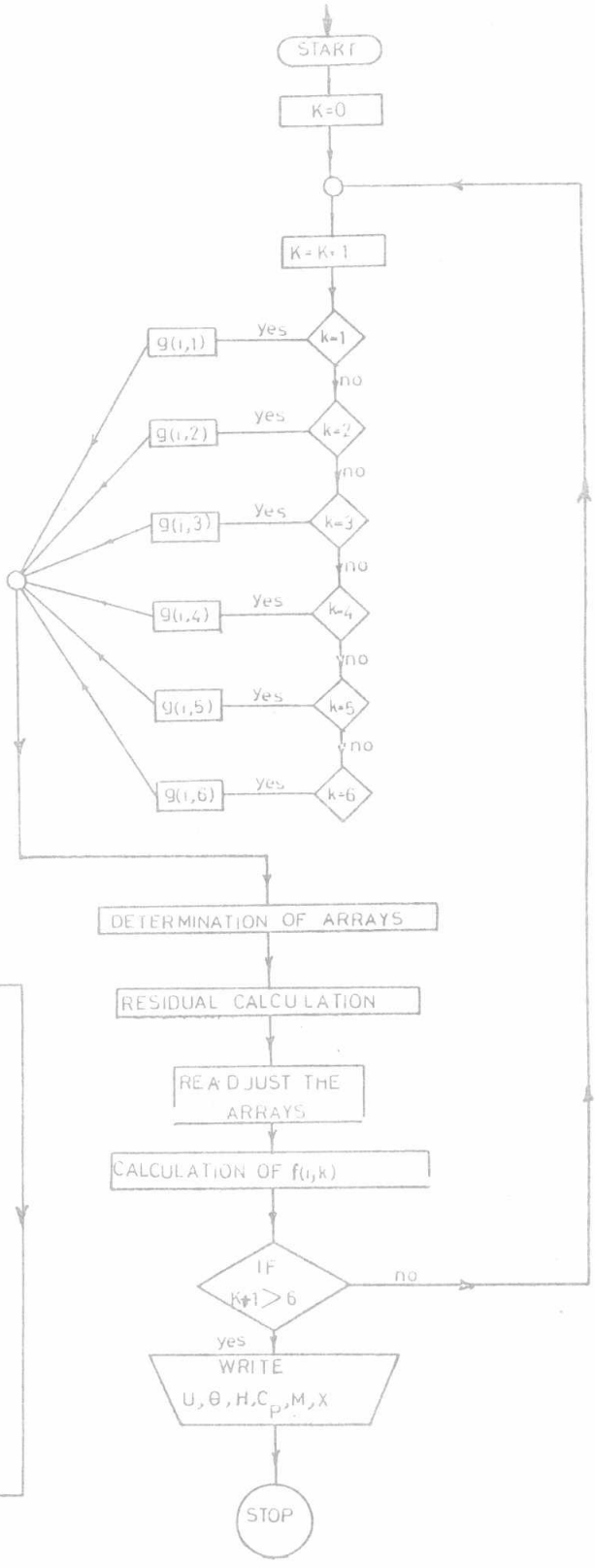

FIG 3 FLOWCHART DIAGRAM OF SUBROUTINE "POTENT"

matrix of the coefficients of $d\theta/dx$, dH/dx, dF/dx should be diagonally dominant, a condition not satisfied in ref. [4]. In the present study the continuity equation was introduced to eliminate the terms containing dU/dx and the stability condition was satisfied (for more details see ref. [8]).

Fig. 2 shows a flow chart of the main program "DUCT" which iterates the potential core flow solution with the boundary layer solution as outlined earlier in 'The Prediction Scheme'.

In Fig. 3 a flow chart of the subroutine "Potent" for solving the 3-D axisymmetric compressible potential core is given, and it shows how the solution progresses as the number of terms (K) in the power series expansions of ψ & B is increased (up to 6 terms).

VERIFICATION OF THE MODEL

Computer Core Size Limitations

The basic difficulty encountered when running the program was that arising from the limited computer core size available. Although the Alexandria University PDP-11 computer used has a core size of 128 K Bites, due to its time sharing nature, the amount of core available for each user is limited to only 28 K Bites. Therefore it was not possible to run programmes which include excessively large arrays. As a result the number of divisions along the duct axis (N) had to be reduced from the planned 100 to only 35 while the number of terms in the power series expnsions (K) was kept at 6. As a result, a larger number of iterations (longer CPU time) was needed to achieve convergence of the solution, i.e. to achieve matching between the potential core flow solution and the boundary layer solution. However, it can be safely stated that the increased number of iterations makes up for the loss of accuracy inflicted by limiting N & K.
This is clearly shown in Figs. 4, 5 & 6, where the theoretical curves

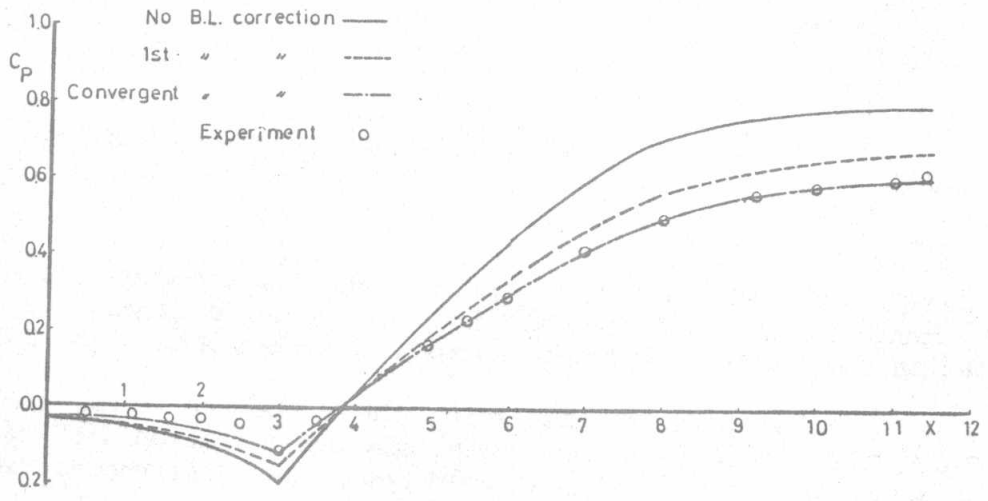

FIG (4) EFFECT OF B.L. CORRECTION FOR 5° CONICAL DIFFUSER

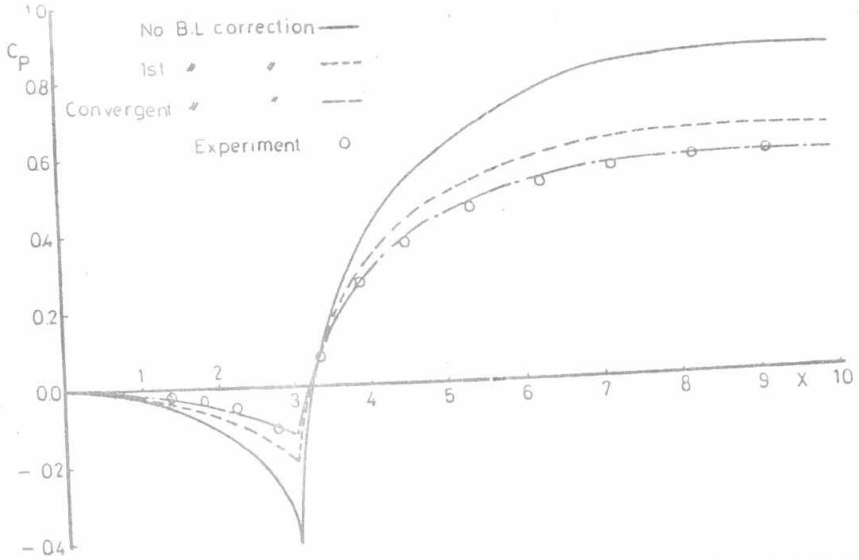

FIG (5) EFFECT OF B.L. CORRECTION FOR 12° CONICAL DIFFUSER

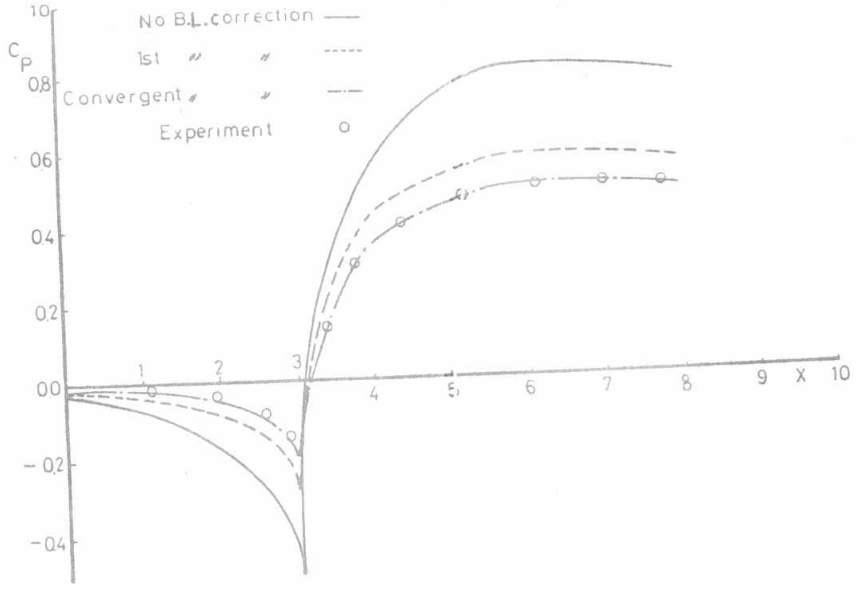

FIG (6) EFFECT OF B.L. CORRECTION FOR 20° CONICAL DIFFUSER

representing the successive iterations gradually approach the experimentally measured points of Ashcroft [6]. As is quite clear from the final iteration there is no appreciable loss in accuracy even with K=4 & N=35.

In Fig. 7 the effects of increasing the number of terms in the power series K from 4 to 6 is studied with only one iteration with the boundary layer solution. Even with one iteration, the differences between the solutions with K=4 and K=6 are not substantial.

6

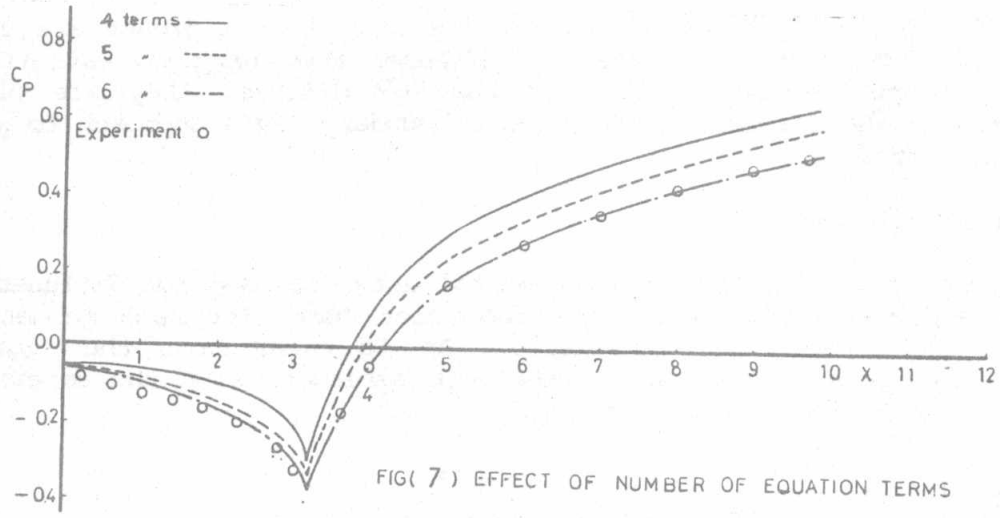

FIG(7) EFFECT OF NUMBER OF EQUATION TERMS

Data Selection for the Verification

In selecting data to verify the model, the comparison with experimental results was intended to consist of two parts:

i Comparison with data that satisfy the assumptions of the theory (or at least most of them) to determine if the theory is adequate and to point out, if possible, its shortcomings.

ii Comparison with data that do not quite satisfy the assumptions of the theory, to determine the maximum useful range of the model.

Satisfactory results from the first comparison provide a domain where the model is established and allow interpolation between measured C_p values. The second comparison indicates the limits for extrapolating beyond the region where C_p has been measured.

Thus the comparison was made using experimental data from references [6] & [7]. In the case of data of Ashcroft, the flow in the diffuser inlet duct was wholly subsonic, while in the case of the data of Kamal the flow was high subsonic following a shock wave-boundary layer interaction, thus diffuser inlet turbulence levels were high. Moreover, in the latter case the transition from the inlet duct to the diffuser cone is always sharp.

The input data requirements of the model are : six duct geometrical parameters and five inlet flow parameters. The duct shape is described using the diffuser angle, area ratio, inlet length, exit length, faired length and degree of fairing. The inlet flow parameters include: the Mach no., Reynold's no., the boundary layer momentum thickness θ & shape parameter H in addition to a turbulence level parameter I_G.

Results of the Comparison Between the Model Predictions and Experimental Data

In the comparisons made in this section, the test cases are grouped

according to the diffuser angle. Results of the 5° diffuser are used to test the flow model, for the 12° diffuser they help to establish the range of applicability while for the 20° diffuser they are used to investigate the feasibility of using a boundary layer approach to predict stalled diffusers.

a- The 5° diffuser

In figures 8 & 9 Ashcroft's experimental data are used for diffusers with faired and sharp transition from the inlet duct. For each geometry two inlet Mach numbers are considered,. As is clear from the figs. the theoretical predictions are in excellent agreement with the experimental values even at the higher Mach number.

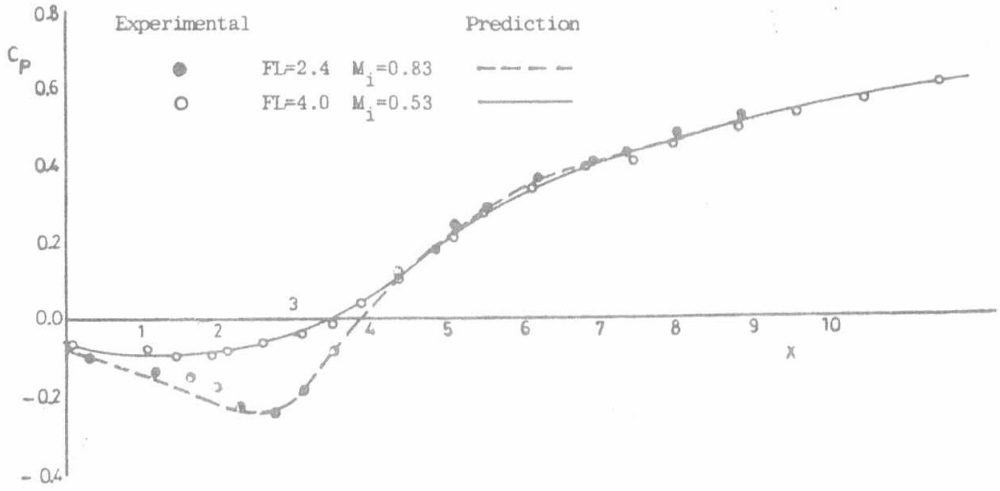

Fig. 8 Comparison with Ashcroft's experimental results : 5° diffuser - faired junction

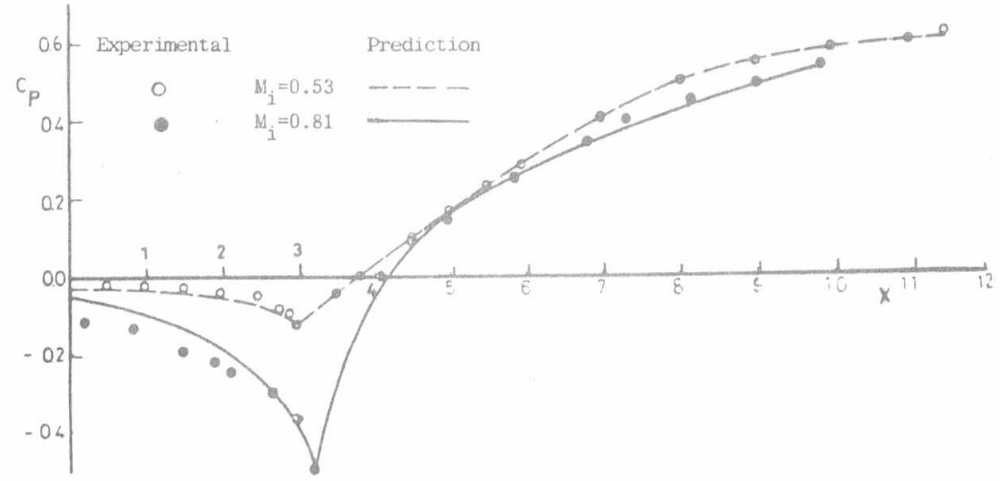

Fig. 9 Comparison with Ashcroft's experimental results : 5° diffuser - sharp junction

The results of the comparison with Kamal's data, fig. 10, including predictions of the growth of the boundary layer parameters θ and H inside the diffuser give extra evidence to the superiority of the model.

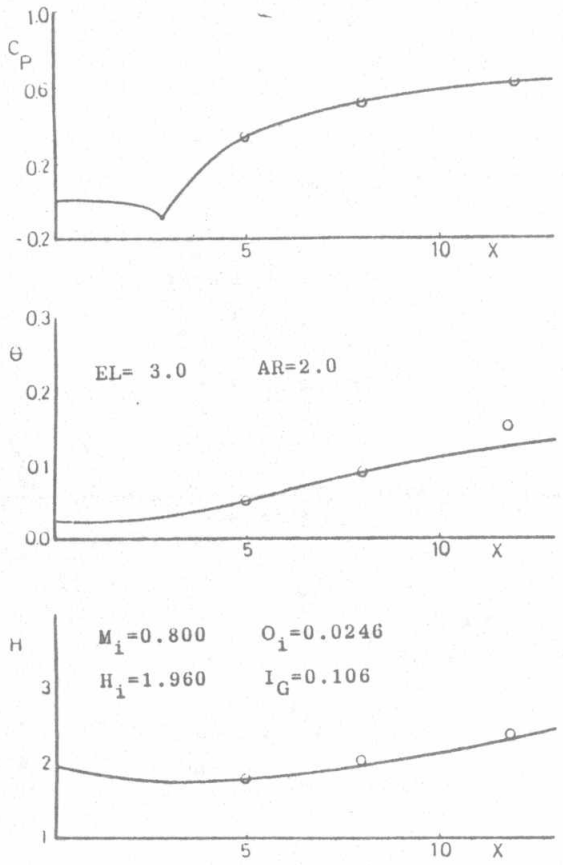

Fig.10 Comparison with Kamal's experimental result : 5° diffuser - sharp junction

b- The 12° diffuser

From the comparison with Ashcroft's experimental data for faired junction (fig. 11) & sharp junction (fig. 12) as well as Kamal's data (fig. 13), it can be generally concluded that, while the theory underestimates the growth of the boundary layer momentum thickness θ & overestimates the H - growth the quantitative prediction of C_p is only adequate. As expected, the predictions become progressively less accurate at the bigger area ratios. Naturally, the effects of the inlet sharp corner are expected to be measurable in the case of the 12° diffuser and are partly responsible for the differences between predictions & data. In the case of the faired junction the departure of experimental results from the theory near diffuser exit is attributed to the onset of stall, or simply to boundary layer separation.

c- The 20° diffuser

Figs. 14 & 15 show a comparison between the theory and experiment for the 20° diffuser with sharp and faired transitions from the inlet duct. The figures indicate a departure of the theoretical C_p-growth from the experimental points very early in the diffuser. Fig. 15 suggests that the overestimation of C_p can be mainly attributed to a serious underestimation of the θ-growth. The excellent predictions of the pressure variation round the diffuser inlet corner, sharp or faired, prove that the early separation is the major source of discrepancy, as is clear from fig. 14.

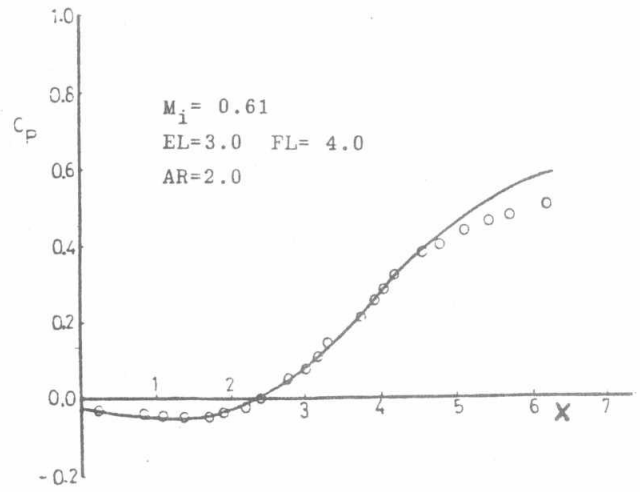

Fig.11 Comparison with Ashcroft's experimental results : 12° diffuser - faired junction

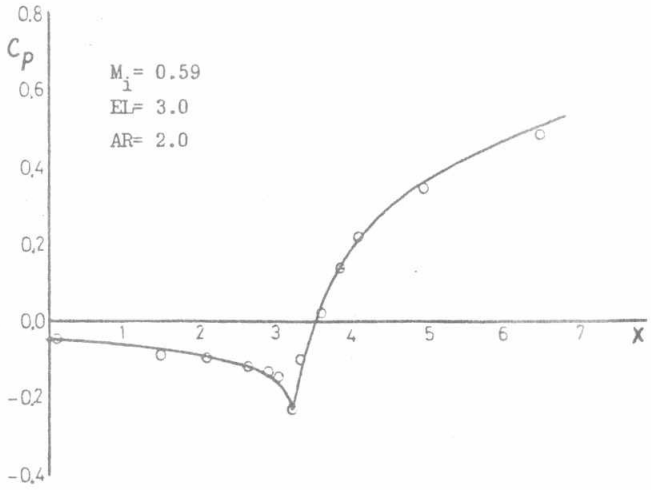

Fig.12 Comparison with Ashcroft's experimental results : 12° diffuser - sharp junction

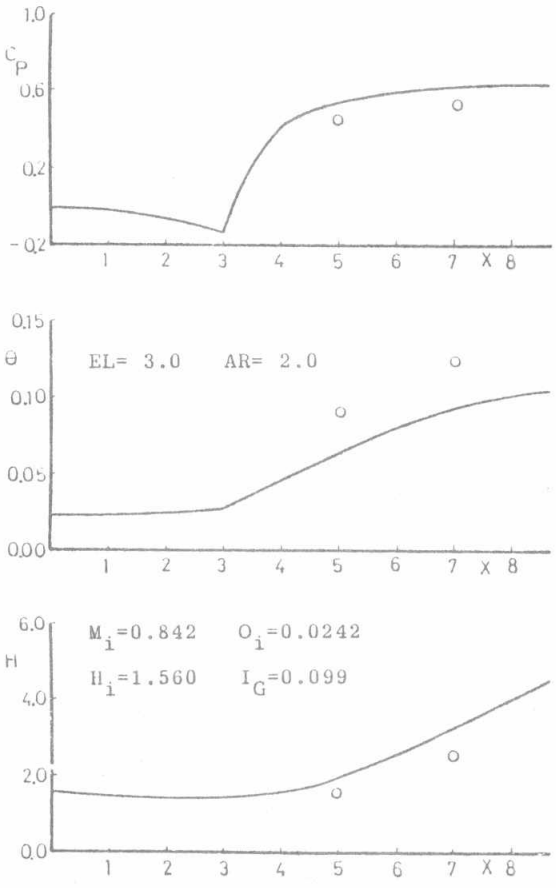

Fig.13 Comparison with Kamal's experimental resuts : 12° diffuser - sharp junction

Indeed, the early separation in the 20° diffuser renders the flow model invalid over most of the diffuser length.

REFERENCES

1. Roberts, D. & Forrester, C. "A Parabolic Computational Procedure for 3-D Flows in Ducts with Arbitrary Cross-sections", Proceedings of the AIAA 16th Aerospace Sciences meeting, Alabama, U.S.A., (Jan. 1978).

2. Briley, W.R. "Numerical Method for Predicting 3-D Steady Viscous Flow in Ducts", Journal of Computational Physics, Vol. 14, pp. 8-28, (1974)

3. Ahmed, N., Konarski, S., Myring, D. & Livesey, J.L., "The Prediction of Flows in General 3-D Passages using Viscous / Inviscid Interaction" Salford University, Internal report FM/27/83 (1983).

4. Livesey, J.L., Ashcroft, D. & Kamal, W.A. "Prediction of Three-Dimensional Axisymmetric Duct Flow", Proceedings of the International Conference on Mechanical Power Engineering (ICMPE), Cairo, pp. VIII. 16.1-VIII. 16.14 (Oct. 1980).

5. Kamal, W.A. & Livesey, J.L. "Prediction of Diffuser Flow and Performance Following a Normal Shock Wave - Turbulent Boundary Layer Interaction", Proceedings of the Symposium on Turbulent Shear Flows, The Pennsylvania State University, pp. 12.1-12.10 (1977).

6. Ashcroft, D.H. "Performance of Conical Diffusers with High Subsonic Entry Mach numbers", Ph.D. Thesis, Manchester University, (1969).

7. Kamal, W.A. "Inlet Flow Structure Effects in Compressible Conical Diffuser Flow", Ph.D. Thesis, Salford University, (1976).

8. Anwar, A.E. "Diffusers for Supersonic Intakes", M.Sc. Thesis, Alexandria University, (Oct. 1983).

NOMENCLATURE

B	density function, = ρ / ρ_o
C_p	wall static pressure recovery coefficient, =$(p-p_o)/(P_o-p_o)$
EL,FL,XL	entry, faired and exit lengths / r_o , see Fig. 1
F	entrainment function
f_i, g_i	functions of (X) difined by equations (5) & (6)
H	boundary layer shape factor, = δ^*/θ
K	number of terms in the power series expansions of ψ and B
M	local Mach number
P & p	local pressure, total & static
r	coordinate normal to duct axis
r_o	duct radius at inlet
U	axial velocity at edge of the boundary layer
X,R	x/r_o , r/r_o
x	coordinate along duct axis
γ	ratio of specific heats
δ^*, θ	displacement and momentum boundary layer thicknesses
ρ	local density
ψ	stream function

Subscripts

o condition at duct inlet section
e condition at edge of boundary layer.

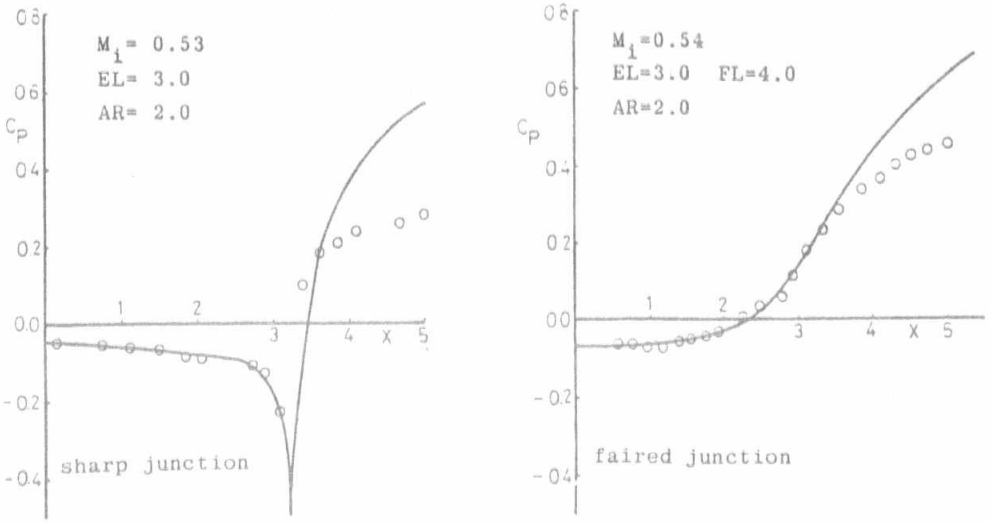

Fig. 14 Comparison with Ashcroft's experimental results : 20° diffuser

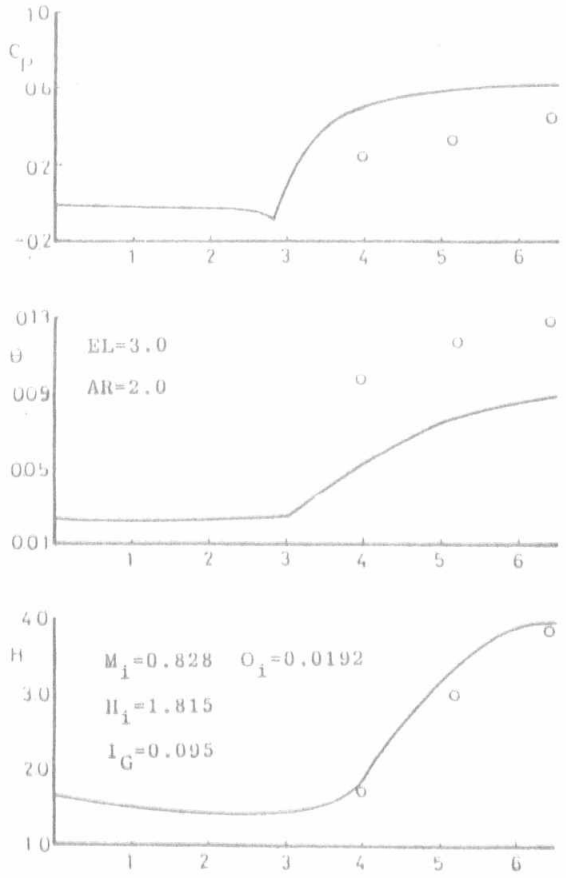

Fig.15 Comparison with Kamal's experimental result :
20° diffuser - sharp junction